Experimental Investigation of the NASA Common Research Model with a Natural Laminar Flow Wing in the NASA Langley National Transonic Facility

Melissa B. Rivers[1], Michelle Lynde[2], Richard Campbell[3], Sally Viken[4], David Chan[5], A. Neal Watkins[6]
NASA Langley Research Center, Hampton, VA 23681

Scott Goodliff[7]
Jacobs Technology, Inc., Hampton, VA 23681

A test of the new NASA Common Research Model with a Natural Laminar Flow (CRM-NLF) semispan wing in the NASA Langley National Transonic Facility (NTF) was completed in October 2018. The main focus of this test was the evaluation of the extent of laminar flow on the CRM-NLF wing at various Reynolds numbers and test conditions. During this test, data were acquired at chord Reynolds numbers from 10 to 30 million and at Mach numbers ranging from 0.84 to 0.86. This investigation provided valuable insight into the necessary procedures for laminar flow testing in the NTF. It also significantly advanced the new carbon-based heating layer technique to improve the quality of transition visualization data from temperature sensitive paint (TSP) in a cryogenic wind tunnel.

I. Nomenclature

b	=	wing span, in.
c	=	wing mean aerodynamic chord, in.
C_D	=	drag coefficient
C_L	=	lift coefficient
C_m	=	pitching moment coefficient referenced to 0.25 of the wing mean aerodynamic chord
M_∞	=	freestream Mach number
q_∞	=	dynamic pressure, psf
Re_c	=	Reynolds number based on mean aerodynamic chord
T_t	=	total temperature
α	=	angle of attack, deg
η	=	fraction of wing semispan
σ	=	standard deviation

II. Introduction

The ability to test models with Natural Laminar Flow (NLF) in a wind tunnel is becoming more and more of a requirement as many aircraft manufacturers are looking to NLF technology to reduce aircraft drag and thus both fuel burn and emissions. The extent of NLF is dependent on many variables, including the turbulence levels in the environment. Typically, wind tunnels have higher turbulence levels compared to the flight environment, thus impacting the extent of laminar flow that can be achieved. This makes wind tunnel testing of NLF configurations particularly challenging, thus encouraging the need for evaluating the tunnel laminar flow testing capability and best practices for laminar flow testing. This includes providing the "cleanest" wind tunnel environment possible, free of

[1] Senior Research Engineer, Configuration Aerodynamics Branch, Mail Stop 267, AIAA Associate Fellow.
[2] Research Aerospace Engineer, Configuration Aerodynamics Branch, Mail Stop 499, AIAA Member.
[3] Senior Research Engineer, Configuration Aerodynamics Branch, Mail Stop 499, AIAA Associate Fellow.
[4] Aerospace Engineer, Configuration Aerodynamics Branch, Mail Stop 499, AIAA Associate Fellow.
[5] Research Aerospace Engineer, Configuration Aerodynamics Branch, Mail Stop 499, AIAA Member.
[6] Research Engineer, Mail Stop 493, AIAA Member.
[7] Test Engineer, Jacobs Technology, Inc., AIAA Member.

contaminants that may cause loss of laminar flow, such as frost, oil, or tunnel particulates, along with a high-quality model surface finish to reduce chance of early boundary layer transition. Over the last couple of years, the NASA Langley National Transonic Facility (NTF) has been focused on improving the capability to obtain NLF data. The NTF was chosen for testing transonic laminar flow concepts as it enables testing scaled models at or near flight Reynolds numbers to better assess the extent of laminar flow. To this end, two risk reduction tests were previously performed. The first risk reduction test utilized the full-span NASA Common Research Model (CRM), designed for $M_\infty = 0.85$, $C_L = 0.5$, at $Re_c = 30$ million. During that test, the wings were painted with a new carbon-based heating layer and a temperature sensitive paint (TSP) layer, which provided a means to measure temperature differences on the wing surface, which relate directly to the existence of laminar flow. The wings were then evaluated at transonic conditions to investigate any potential for NLF. The flow visualization data obtained from that test provided information that was then used for the follow-on test that utilized an NLF wing that had been previously tested in the NTF. That second wind tunnel test provided more insight into the best methods for NLF testing, including the best formula for the TSP and the best method to use for a heating layer. Those insights were then implemented during this test of a new NLF wing in the NTF.

At the same time those risk reduction tests were being performed, a new CRM wing was being designed to experimentally validate a new NLF technology called Crossflow Attenuated NLF (CATNLF). CATNLF technology enables a significant extent of NLF on wings with sweep and Reynolds number typical of transports by using geometry shaping to obtain surface pressures that delay boundary layer transition due to crossflow. This newly designed CRM-NLF wing (Fig. 1), with leading-edge sweep of 37.3° (outboard of $\eta = 0.2$ measured from fuselage centerline), for a cruise design condition of $M_\infty = 0.85$, $C_L = 0.5$, and $Re_c = 30$ million. Based on a critical N-factor of 10, the wing is estimated to have 56% laminar flow on the wing upper surface at the design condition. Once the model of the CRM-NLF wing design (developed by Lynde and Campbell [1]) was fabricated, the testing in NTF had three specific goals: (1) to validate the CATNLF design methodology and analysis tools, (2) to characterize the NTF laminar flow testing capabilities, and (3) to establish best practices for laminar flow wind tunnel testing. This paper will only briefly touch on these goals but a companion paper will cover them in depth.

III. Facility Description

The NTF [2] is a unique national facility (Fig. 2) that enables testing of aircraft configurations at conditions ranging from subsonic to low supersonic speeds at Reynolds numbers up to full-scale flight values. The NTF is a conventional, closed-circuit, continuous-flow, fan-driven wind tunnel capable of operating in either dry air at warm temperatures or pure nitrogen from warm to cryogenic temperatures. Elevated pressures in combination with cryogenic temperatures enable testing to the highest Reynolds numbers. The test section is 8.2 by 8.2 by 25 ft. and has a slotted floor and ceiling. In addition, turbulence is reduced by four antiturbulence screens in the settling chamber and a contraction ratio of 14.95-to-1 from the settling chamber to the nozzle throat. Fan-noise effects are minimized by acoustic treatment both upstream and downstream of the fan. Thermal insulation resides inside the pressure shell to aid in maintaining tunnel temperature and thus minimizes energy consumption. Figure 3 is a sketch of the NTF tunnel circuit, including the location of the Sidewall Model Support System (SMSS) used for semispan model testing.

The NTF has an operating pressure range of approximately 15 to 120 psia, a temperature range of -260 to +120°F, and a Mach number range of 0.2 to 1.2. The maximum unit Reynolds number is 146×10^6 per foot at Mach 1. When the tunnel is operated cryogenically, heat is removed by the evaporation of liquid nitrogen, which is sprayed into the tunnel circuit upstream of the fan. During this operational mode, venting is necessary to maintain a constant total pressure. When air is the test gas, heat is removed from the system by a water-cooled heat exchanger at the upstream end of the settling chamber. For this investigation, the tunnel was operated entirely in nitrogen mode. Further tunnel details and facility information are provided in Ref. 3.

The original design of the NTF did not include a provision for semispan testing. In the 1990s, when the need for low-speed, high-lift configuration testing at higher Reynolds numbers became apparent, the semispan testing ability was added to the NTF [4-6]. In 2007, another enhancement was made that allowed semispan transonic cruise testing at the NTF. With testing of several entries of the Fundamental Aerodynamic Subsonic Transonic Modular Active Control (FAST-MAC) model [7-10] and the Lockheed Martin Speed Agile model [11,12], semispan testing has continued to be improved at the NTF.

Semispan models are installed on the tunnel sidewall of the NTF and attach to the external Force Measurement System (FMS) inside the SMSS, where the NTF-117S force and moment strain gauge balance is located. The SMSS is installed in the far-side wall of the test section, which supports the model in approximately the middle of the test section. To keep the metric model parts from being subjected to test section wall boundary layer effects, a 2-inch standoff is used and a labyrinth seal is used to preserve the metric break. With this type of testing, there is a large

temperature gradient between the test section temperature (can be as cold as -150ºF for this test) and the balance temperature, which is nominally held at 100ºF, as shown in Fig. 4. Due to the large pressure gradients that can be established by the aerodynamics of the model, cold air from the tunnel test section can be ingested into the balance cavity and heated air can be pulled out from the SMSS into the test section. To guard against this, the SMSS provides a heated enclosure that maintains a stable temperature for the balance by using convective heat transfer provided by the closed loop Balance Cavity Recirculation System (BCRS). Figure 5 shows how the BCRS constantly circulates heated air throughout the balance cavity and around the balance to condition any cold air flow ingestion from the tunnel test section.

IV. Experimental Setup

A. Model Description

The model for this investigation was a newly designed CRM-NLF wing that was mated to an existing semispan fuselage. The new CRM-NLF wing was designed by Campbell and Lynde [1] as mentioned above. The contract to fabricate this new design was awarded to Advanced Technology Incorporated (ATI) in Newport News, VA. The model was built to withstand the wide temperature range of the NTF (-250ºF to 120ºF). The surface finish for the new hardware was required to be 16 micro-inches root mean square (RMS) or below. The swept wing leading-edge region is most important for delaying boundary layer transition due to crossflow and thus obtaining extents of laminar flow, so the surface contour of the wing leading edge was the most critical. The new wing was fabricated out of cryogenically acceptable steel, Vascomax C250.

The new semispan wing has an aspect ratio of 9.0 and model semispan of 60.15 in. The reference area of the new wing is 5.584 ft^2 while the reference length is 14.34 in. The fuselage length is 10.71 ft. A sketch of the key locations on the model as well as the locations of the balance moment center (BMC) and model moment center (MMC) are shown in Fig. 6. A picture of the model installed in the NTF is shown in Fig. 7.

B. Instrumentation

1. Balance

For semispan testing in the NTF, the NTF-117S balance is used to measure force and moment data. This balance is a large five-component strain gauge balance that is mounted inside the SMSS. The balance is 16 in. in diameter and 26 in. in length with resistance temperature detectors (RTDs) around the balance to monitor temperature stability during test operations. Table 1 shows the maximum load range for this balance.

2. Wing surface & fuselage static pressures

The CRM-NLF wing is instrumented with 230 static pressure orifices that are arranged in nine streamwise rows across the span (η = 0.163, 0.252, 0.370, 0.460, 0.550, 0.640, 0.730, 0.820 and 0.910). The layout of the pressure rows is shown in Fig. 8. To avoid disturbing the leading-edge flow across the entire wing that could lead to turbulent wedges and loss of laminar flow, leading edge pressure taps were only present at four span stations, namely η = 0.163, 0.370, 0.640 and 0.820.

The fuselage of this model has 14 static pressure orifices that were connected during the test to monitor any flow inside the fuselage. The back of the fuselage also contains keel plates that are installed to seal and block any flow from entering the fuselage. Some of these plates and the back side of the fuselage are also instrumented with static pressure taps in order to measure and monitor the flow between the standoff and the fuselage. Locations of the fuselage and keel plate pressures are shown in Fig. 9.

3. Fouling strips

Model fouling circuits were installed between the metric fuselage parts and the nonmetric standoff to ensure there was no metric to nonmetric fouling during the test. A total of four fouling circuits were used: one on the upper nose section, one on the lower nose section, one on the upper tail section, and one on the lower tail section. The balance mechanism had three fouling circuits installed: one on the top hat seal, one on the labyrinth seal, and a third on the flow blocking collar.

4. Carbon-based heating layer leads

The model was fabricated to accommodate eight electrical leads that were used to provide power for the carbon-based heating layer for the flow visualization technique. These wires were 18-gauge wires, which were run internal to the wing to provide a uniform level of current across the entire wing. The wires were terminated on the wing surface (upper and lower), and the leads exited the wing through the root where they were connected to the heating system power supplies.

5. Transition scheme

One boundary layer transition scheme was used for the entire test. Self-adhesive trip dots were applied only to the lower surface of the wing at 5% chord. Epoxy trip dots were applied to the fuselage nose. The trips applied to the nose were 0.004 in. in height and the trips applied to the lower surface of the wing were 0.002 in. in height. The specific locations of the trips are shown in Fig. 10. All of the dots had a diameter of 0.05 in. and were spaced 0.10 in. apart (center to center).

C. Temperature Sensitive Paint and Carbon-Based Heating Layer

TSP was employed for transition location determination at the NTF due to its ability to detect global surface temperature changes at cryogenic conditions. TSP is typically composed of a gas impermeable binder in which luminescent dye molecules are immobilized [13]. With a suitable binder, changes in the luminescent output of the dye are solely due to changes in temperature (i.e., thermal quenching). The temperature change in transition is due to the difference in heat transfer between laminar flow and turbulent flow. However, depending on the flow conditions of the facility, this temperature change is typically on the order of 0.1 degree, which usually needs to be enhanced to visualize with TSP. Traditionally, this has been done by introducing a temperature step into the tunnel. This is usually accomplished by rapidly changing the liquid nitrogen injection rate in the tunnel in either a positive (less nitrogen flow) or a negative (more nitrogen flow) temperature direction. While quite effective in enhancing the temperature difference on the model due to transition, this can add a significant cost in terms of data acquisition time and facility operation. In addition, there can also be a significant change in the local flow conditions during the step.

Recently, however, work has been presented combining TSP with a carbon-based heating layer [14-16]. The heating layer acts as a resistive heater that can locally increase the temperature on the model surface when current is flows through it. This provides a means to apply a temperature step directly to the model (as opposed to the flow), greatly decreasing the data acquisition time (as the tunnel does not need to recover after each temperature step) and stability in the flow conditions. Optimization of the technique has allowed demonstrations down to -262˚F on smaller airfoil shapes.

D. Test Conditions

The investigation, conducted over a few months, provided force and moment, surface pressure, model deformation, and surface flow transition visualization data. Testing was conducted at 10 to 30 million Reynolds number. All Reynolds number data presented in this paper are based on mean aerodynamic chord. The Reynolds number of 15 million was the main focus of the laminar flow study, and all of the Reynolds number data were used to provide an assessment of Reynolds number effects. The data were collected at temperatures near -150ºF, -53ºF, and 40ºF.

All data presented in this paper were obtained at freestream Mach numbers ranging from 0.84 to 0.86, with the primary focus being at 0.86 for most of the test. Data were generally obtained over an angle-of-attack range from 1.5° to 3.5° at all Reynolds numbers.

As mentioned above, one of the main objectives of this test was to verify the ability to perform laminar flow testing in the NTF. To accomplish this goal, TSP was used on the model to visualize the transition location on the wing. Two methods were used during this test to obtain TSP data: use of the carbon-based heating layer and the more traditional temperature step method. More information on the results of the TSP data will be provided in a companion paper entitled "**Preliminary Results from an Experimental Assessment of a Natural Laminar Flow Design Method" by Lynde et al.**

Model deformation measurements were also obtained at the end of the test campaign. Since an effective correlation of computational and experimental data will be directly tied to how well the computational and experimental model geometries match one another, it is important to obtain an accurate definition of the model geometry as tested under aerodynamic loads. In order to obtain this information, a video model deformation measurement technique has been developed and employed multiple times at the NTF. This system was used in the current investigation to obtain wing deflection and twist measurements due to aerodynamic loading, but the data are not presented herein.

V. Results and Discussion

A. Data Repeatability

For any wind tunnel test, it is important to assess data accuracy and/or data repeatability. To obtain the most reliable assessment of data repeatability, it is best to have the repeat runs distributed widely throughout the duration of the investigation. Over the course of the test, repeat runs were obtained on the same day and over the course of the test. Note, the focus of this test was not on acquiring force and moment data for performance assessment, but more on gathering surface pressure data and flow visualization data to assess extent of NLF at the test conditions The

repeatability data from the test are presented in Figs. 11-19. Delta coefficient data are presented versus angle of attack for each condition. The delta coefficient data represent the difference between the coefficient value measured and the average value of the coefficient for all of the runs at that particular angle of attack. These delta coefficient, or residual, data show the level of variation in the repeat runs. The solid lines shown on each plot indicate the 2-sigma limits based on all the data across the angle-of-attack range. These figures show that all of the residual data fall within the 2-sigma limits, and Table 2 gives the actual residual values, which are one drag count or less and four lift counts or less for each Reynolds number tested.

B. Reynolds Number Effects

During this test, data were taken at Reynolds numbers from 10 million up to 30 million by varying the temperature to examine the Reynolds number effects on this new wing. The Reynolds number effects at $M_\infty = 0.86$ and $T_t = 40°F$ are shown in Fig. 20. As the Reynolds number is increased, the C_L decreases, the C_m increases, and very little difference is seen in C_D. The Reynolds number effects at $T_t = -53°F$, shown in Fig. 21, indicate the C_L again decreases and the C_m increases with increasing Reynolds number. At this temperature, the C_D decreases from $Re_c = 12.5$ million to 15 million but then increases when Re_c increases to 17.5 million and decreases again when the Re_c increases to 20 million. At $T_t = -153°F$, the C_L and C_D both decrease and the C_m once again becomes less nose down as the Reynolds number increases, as seen in Fig. 22. Typically, as Reynolds number increases, the skin friction drag decreases, which in turn means the total drag should decrease and effective camber increases. This typically results in an increase in lift at a given angle-of-attack, and at a given C_L, the pitching moment should be more negative. None of the data at any of the three temperatures presented follow these trends. This break in trend may be explained by a greater extent of laminar flow at the lower Reynolds numbers, which in turn could cause a thinner boundary layer at the trailing edge of the upper surface than the higher Reynolds numbers. This behavior is being investigated further.

C. Aeroelastic Effects

Another effect that was investigated during this test was the aeroelastic effects on this new wing. Typically, drag decreases with increasing dynamic pressure, which corresponds to a decrease in lift attributable to a small wing twist with the wingtip leading edge deflected downward resulting in a decreased local angle of attack. This would also manifest with an increase in the pitching moment. Figures 23-25 show the aeroelastic effects on this wing at Re_c = 12.5, 15 and 20 million, respectively. In these figures, a closeup view of the plots are given on the right-hand side of the figures. Figure 23 shows that for Re_c =12.5 million, an increase in q_∞ gives a lower C_L, little to no change in C_D, and an increase in pitching moment. Figure 24 indicates that for Re_c = 15 million, an increase in q_∞ gives a lower C_L, an increase in C_D, and a little change in pitching moment. Figure 25 shows the aeroelastic effects for Re_c = 20 million. Again, an increase in q_∞ gives a lower C_L, little to no change in C_D, and an increase in pitching moment similar to the Re_c = 12.5 million data. All of the data shown follow the expected aeroelastic trends for lift, drag, and pitching moment except at Re_c = 15 million where the drag increases. The cause of this discrepancy is unknown at this time and is also being investigated further.

VI. Conclusions

A successful investigation of the new Common Research Model with Natural Laminar Flow wing has been completed in the National Transonic Facility. The NTF was chosen for testing transonic laminar flow concepts, as it enables testing scaled models at or near flight Reynolds numbers to better assess the extent of laminar flow. The three specific goals for the NTF investigation were to validate the CATNLF design methodology and analysis tools, to characterize the NTF laminar flow testing capabilities, and to establish best practices for laminar flow wind tunnel testing. To address these goals, data were obtained at chord Reynolds numbers from 10 to 30 million at Mach numbers from 0.84 to 0.86, with $M_\infty = 0.86$ being the main focus. Force and moment, surface pressure, and surface flow visualization data were obtained, but only the force and moment data are presented herein. Repeatability, Reynolds number effects, and aeroelastic effects have been assessed. Most of the data shown fall within the 2-sigma limits for repeatability, while increases in chord Reynolds number do not follow the normal Reynolds number effect trends. This result is being investigated further, but may be due to a greater extent of laminar flow at the lower Reynolds numbers, which in turn could cause a thinner boundary layer at the trailing edge of the upper surface than the higher Reynolds numbers. The aeroelastic effects did follow expected trends except at Re_c = 15 million, which is also being investigated further.

Acknowledgments

This research was funded by the Advanced Air Transport Technology (AATT) Project. The authors would like to gratefully acknowledge the efforts of the NTF staff for the support provided during this test.

References

[1]Lynde, M. N., and Campbell, R. L., "Computational Design and Analysis of a Transonic Natural Laminar Flow Wing for a Wind Tunnel Model," AIAA-2017-3058, June 2017.

[2]Gloss, B. B., "Current Status and Some Future Test Directions for the US National Transonic Facility. Wind Tunnels and Wind Tunnel Test Techniques," Royal Aeronautical Society, 1992, pp. 3.1-3.7.

[3]Fuller, D. E., "Guide for Users of the National Transonic Facility," NASA TM-83124, 1981.

[4]Gatlin, G. M., Parker, P. A., and Owens, L. R., "Development of a Semi-Span Test Capability at the National Transonic Facility," AIAA Paper 2001-0759, AIAA, January 2001.

[5]Gatlin, G. M., Parker, P. A., and Owens, L. R., "Advancement of Semispan Testing at the National Transonic Facility," Journal of Aircraft, Vol. 39, No. 2, Mar-Apr 2002, pp. 339-353.

[6]Gatlin, G. M., Tomek, W. G., Payne, F. M., and Griffiths, R. C., "Recent Improvements in Semi-Span Testing at the National Transonic Facility (Invited)," AIAA Paper 2006-0508, AIAA, January 2006.

[7]Milholen-II, W. E., Jones, G. S., and Cagle, C. M., "NASA High-Reynolds Number Circulation Control Research - Overview of CFD and Planned Experiments (Invited)," AIAA Paper 2010-344, AIAA, January 2010.

[8]Milholen-II, W. E., Jones, G. S., Chan, D. T., and Goodliff, S. L., "High-Reynolds Number Circulation Control Testing in the National Transonic Facility (Invited)," AIAA Paper 2012-0103, AIAA, January 2012.

[9]Milholen-II, W. E., Jones, G. S., Chan, D. T., Goodliff, S. L., Anders, S. G., Melton, L. P., Carter, M. B., Allan, B. G., and Capone, F. J., "Enhancements to the FAST-MAC Circulation Control Model and Recent High-Reynolds Number Testing in the National Transonic Facility," AIAA Paper 2013-2794, AIAA, June 2013.

[10]Chan, D. T., Milholen-II, W. E., Jones, G. S., and Goodliff, S. L., "Thrust Removal Methodology for the FAST-MAC Circulation Control Model Tested in the National Transonic Facility," AIAA Paper 2014-2402, AIAA, June 2014.

[11]Zeune, C. H., "An Overview of the Air Force's Speed Agile Concept Demonstration Program," AIAA Paper 2013-1097, AIAA, January 2013.

[12]Hooker, J. R., Wick, A. T., Zeune, C. H., Jones, G. S., and Milholen-II, W. E., "Design and Transonic Wind Tunnel Testing of a Cruise Efficient STOL Military Transport," AIAA Paper 2013-1100, AIAA, January 2013.

[13]Liu, T. and Sullivan, J. Pressure and Temperature Sensitive Paints (Experimental Fluid Dynamics); Springer-Verlag Berlin, Germany, 2004, pp. 8-11.

[14]Klein, C., Henne, U., Sachs, W., Beifuss, U., Ondrus, V., Bruse, M., Lesjak, R., and Löhr, M., "Application of Carbon Nanotubes (CNT) and Temperature-Sensitive Paint (TSP) for the Detection of Boundary Layer Transition," *52nd AIAA Aerospace Sciences Meeting*, National Harbor, MD, 2014; AIAA 2014-1482.

[15]Klein, C., Henne, U., Sachs, W., Beifuss, U., Ondrus, V., Bruse, M., Lesjak, R., Löhr, M., Becher, A., and Zhai, J., "Combination of Temperature-Sensitive Paint (TSP) and Carbon Nanotubes (CNT) for Transition Detection," *53rd AIAA Aerospace Sciences Meeting*, Kissimmee, FL, 2015; AIAA 2015-1558.

[16]Goodman, K.Z., Lipford, W.E., and Watkins, A.N., "Boundary-Layer Detection at Cryogenic Conditions Using Temperature Sensitive Paint Coupled with a Carbon Nanotube Heating Layer," *Sensors*, Volume 16, No. 12, 2016, 2062.

Table 1. Maximum load range for NTF-117S balance.

Beam	Calibration Load Range (lbs) or (in-lbs)	Accuracy Load (95% Conf.)
Normal	± 12,000	± 6.00 lbs
Axial	± 1,800	± 2.52 lbs
Pitch	± 90,000	± 144 in-lbs
Roll	± 669,000	± 803 in-lbs
Yaw	± 100,350	± 90.3 in-lbs

Table 2. 2-Sigma Repeatability data for CRM-NLF wing.

Re_c, million	T_t, °F	ΔC_D	ΔC_L
10	40	0.0001	0.003
12.5	40	0.0001	0.003
12.5	-53	0.0001	0.002
15	40	0.0001	0.004
15	-53	0.0000	0.003
17.5	-53	0.0001	0.002
20	-53	0.0001	0.001
20	-153	0.0001	0.001
30	-153	0.0000	0.000

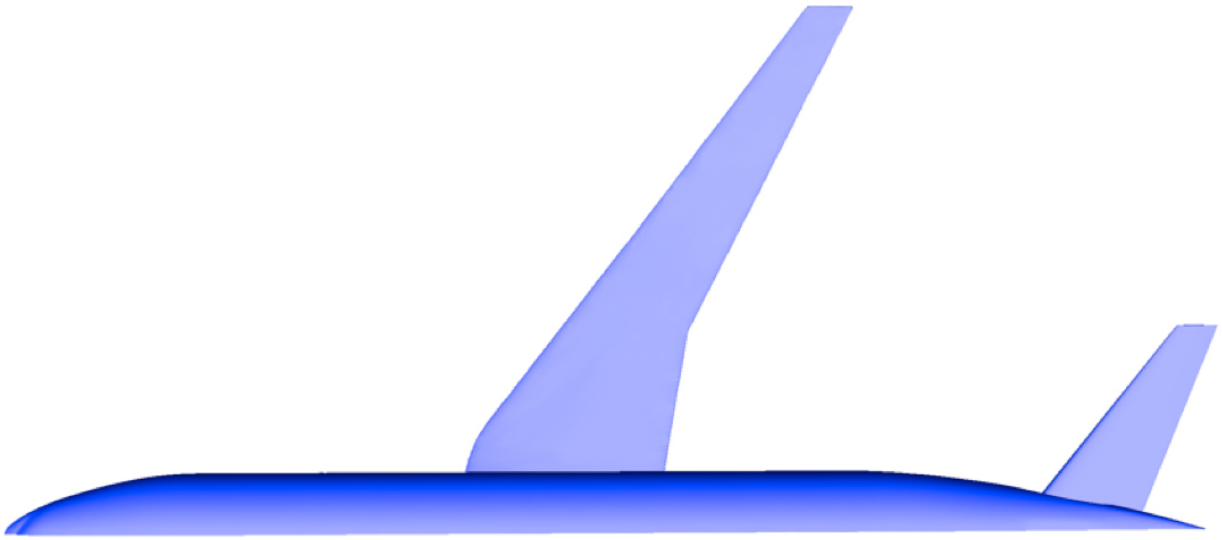

Fig. 1. Planform view of the CRM-NLF design configuration.

Fig. 2. Aerial view of the National Transonic Facility.

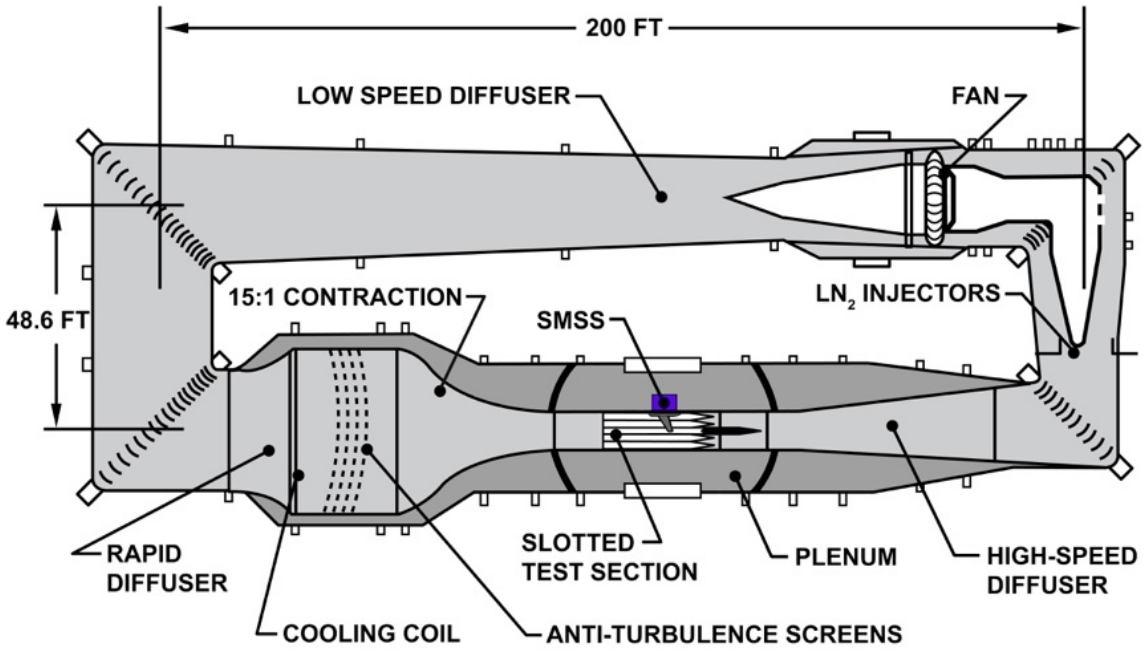

Fig. 3. Sketch of the National Transonic Facility tunnel circuit.

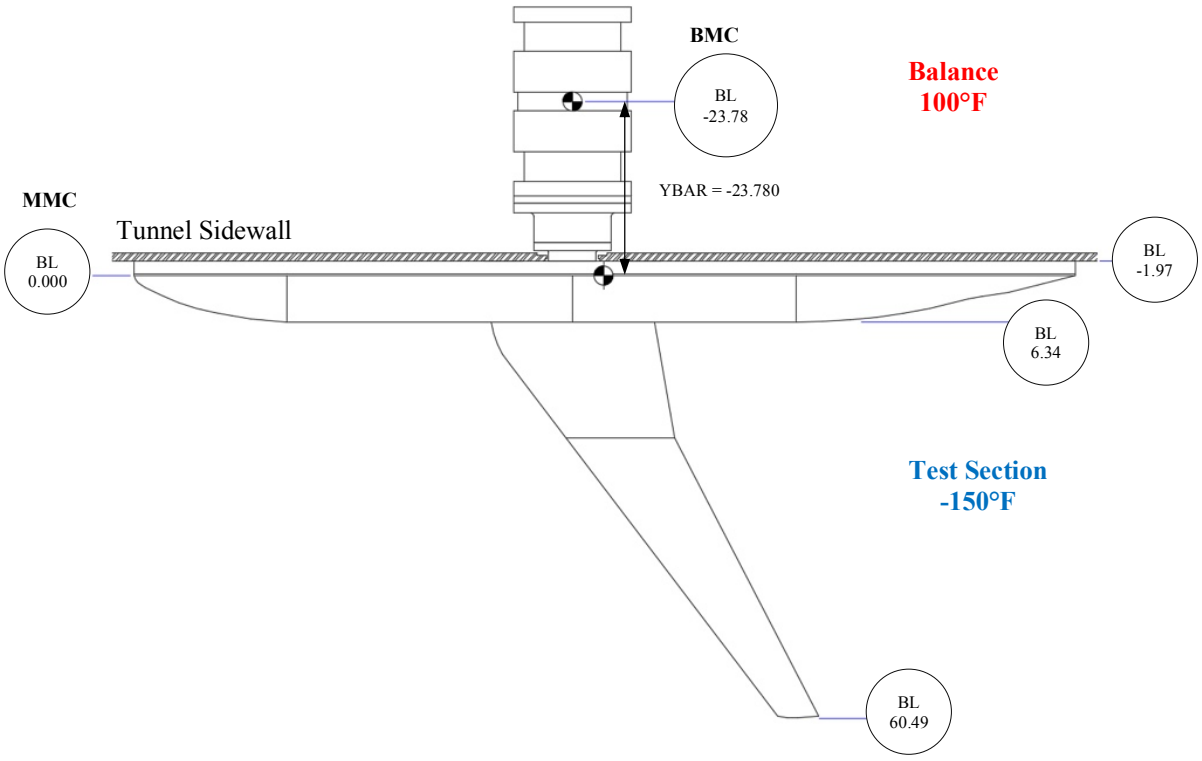

Fig. 4. Top view of the NASA Common Research Model with Natural Laminar Flow wing attached to the NTF external force measurement system.

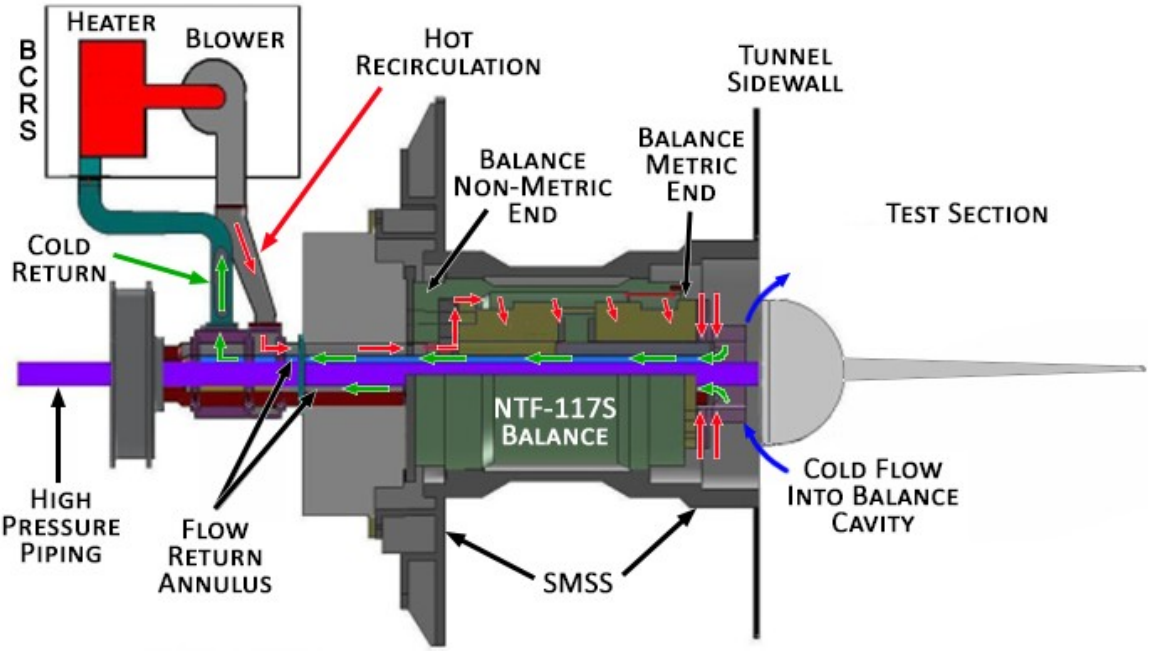

Fig. 5. Balance Cavity Recirculation System used for semispan testing at the NTF.

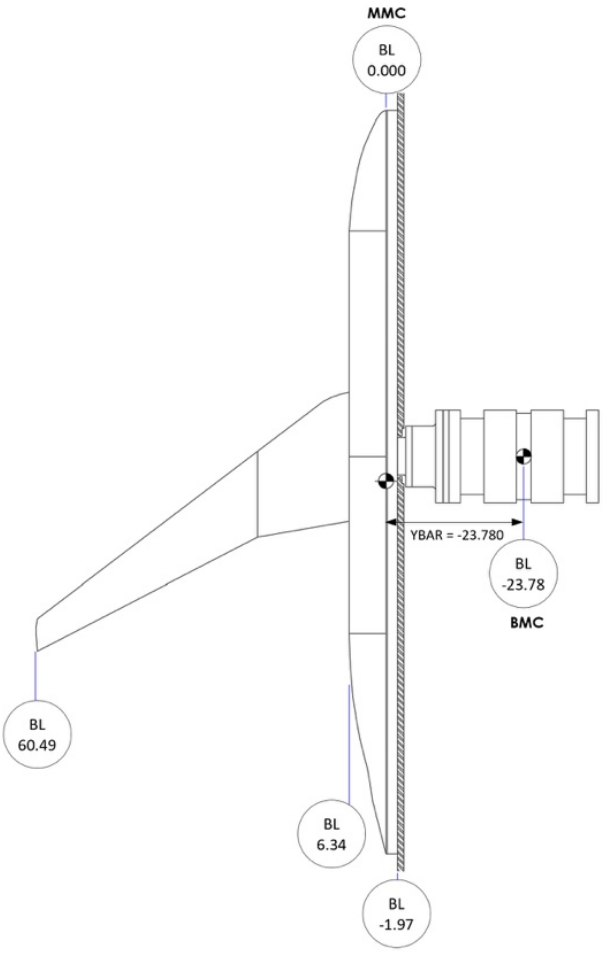

a) Side view

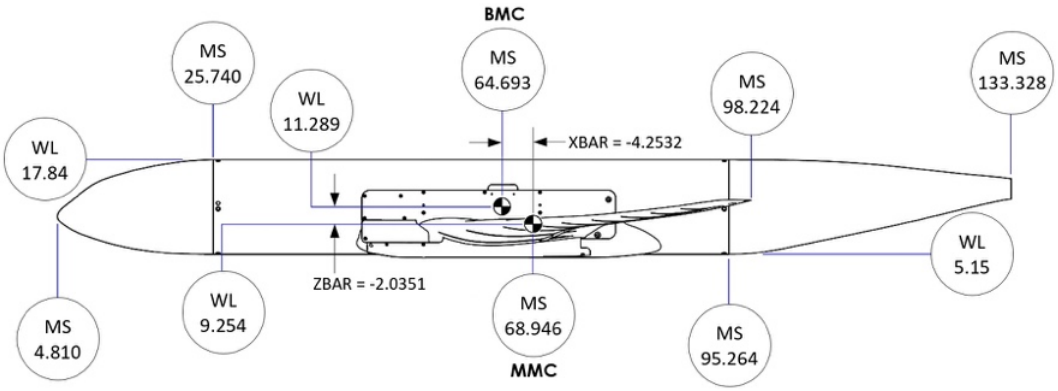

b) Planform view

Fig. 6. Sketches of reference locations of the NASA Common Research Model with Natural Laminar Flow wing model. All dimensions are given in inches.

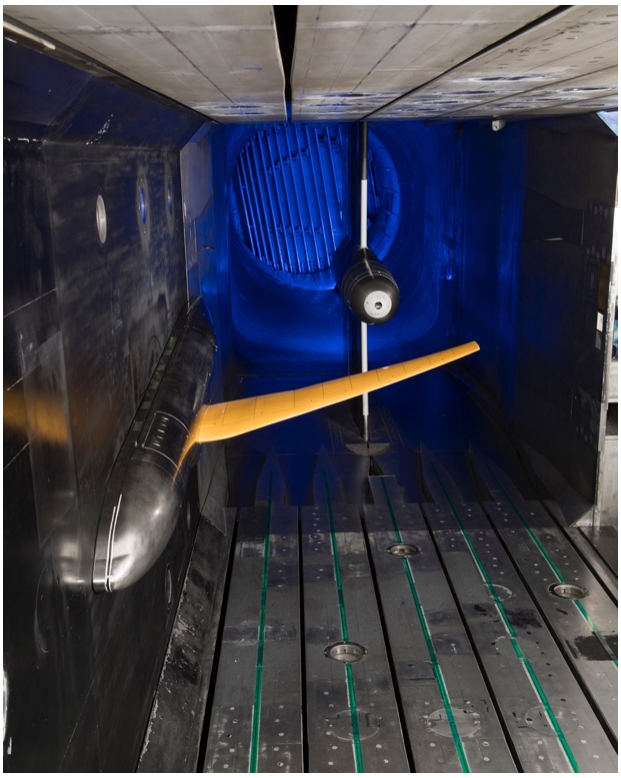

Fig. 7. Photo of the Common Research Model with Natural Laminar Flow wing in the National Transonic Facility.

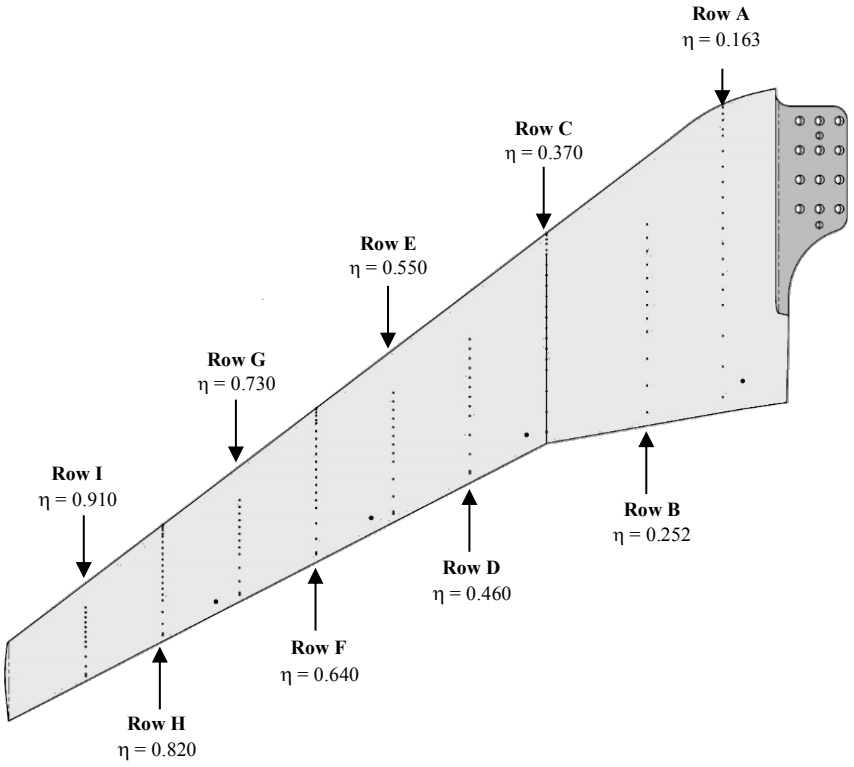

Fig. 8. Location of pressure rows on the CRM-NLF semispan wing.

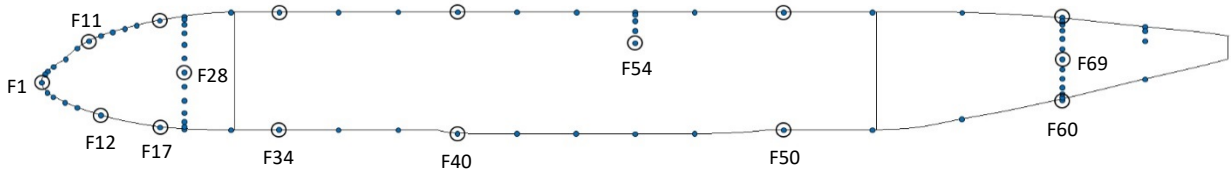

a) Fuselage pressure locations

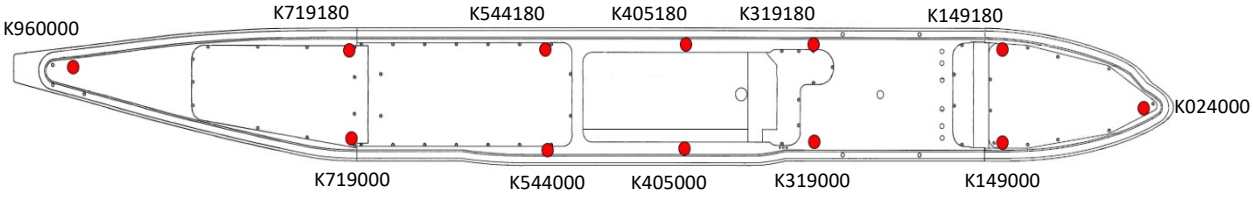

b) Keel pressure locations

Fig. 9. Location of fuselage and keel pressures on the CRM-NLF semispan model.

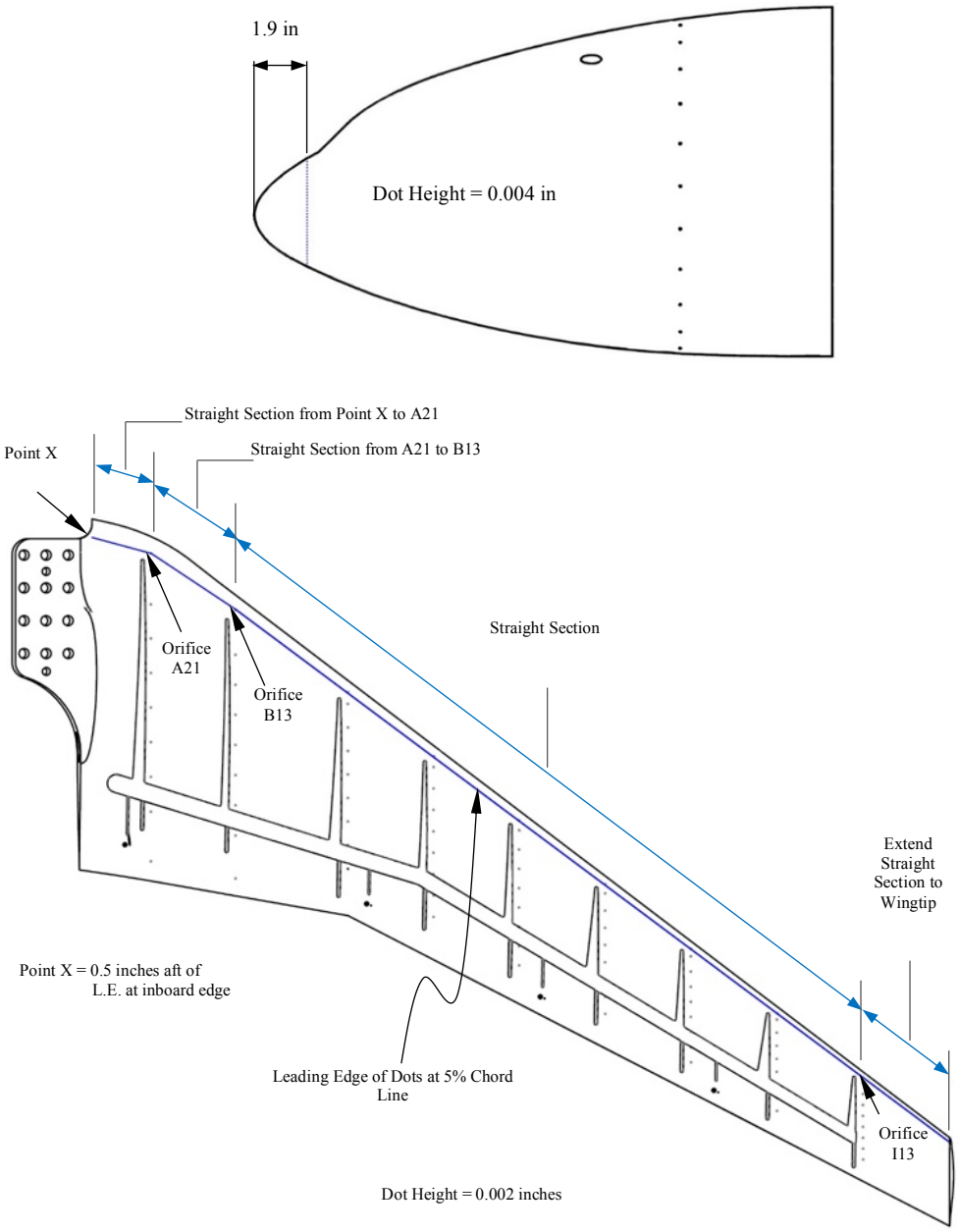

Fig. 10. Location of trip dots on the fuselage nose and the lower surface of the CRM-NLF semispan wing.

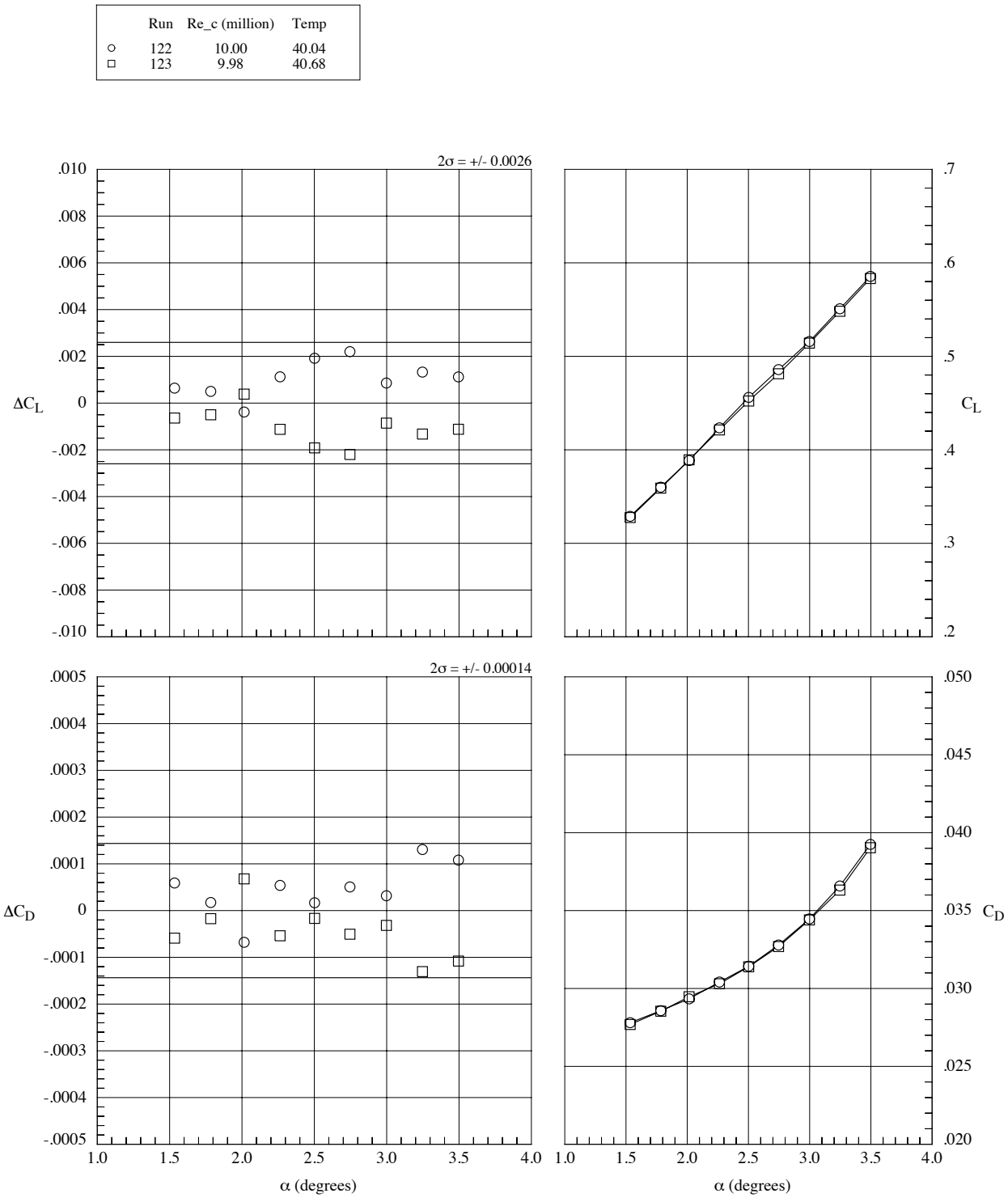

Fig. 11. Data repeatability, $M_\infty = 0.86$, $Re_c = 10$ million, $T_t = 40^\circ F$, $q_\infty = 1183$ psf. Solid line indicates 2-sigma limits based on the residual data.

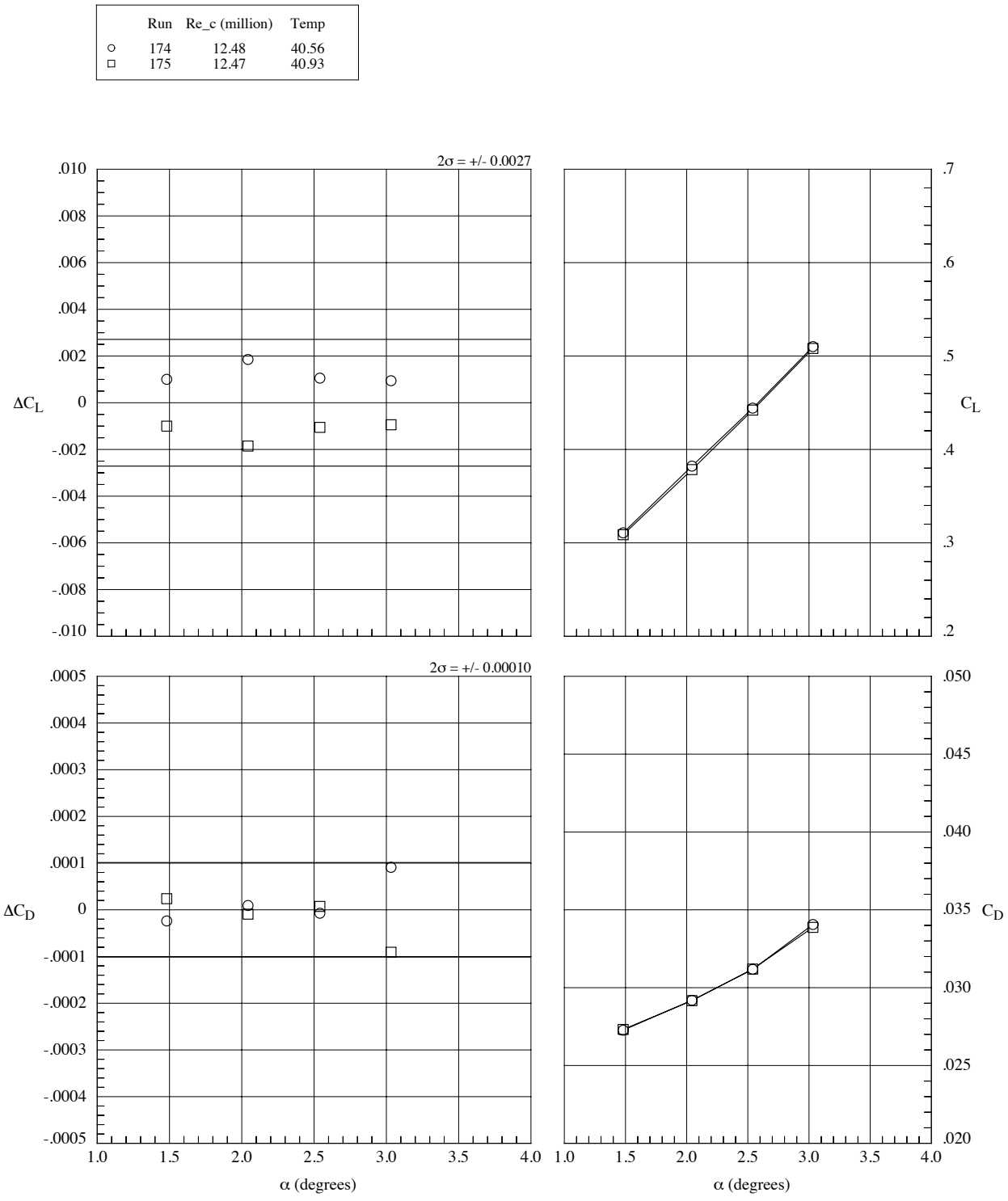

Fig. 12. Data repeatability, $M_\infty = 0.86$, $Re_c = 12.5$ million, $T_t = 40^\circ F$, $q_\infty = 1479$ psf. Solid line indicates 2-sigma limits based on the residual data.

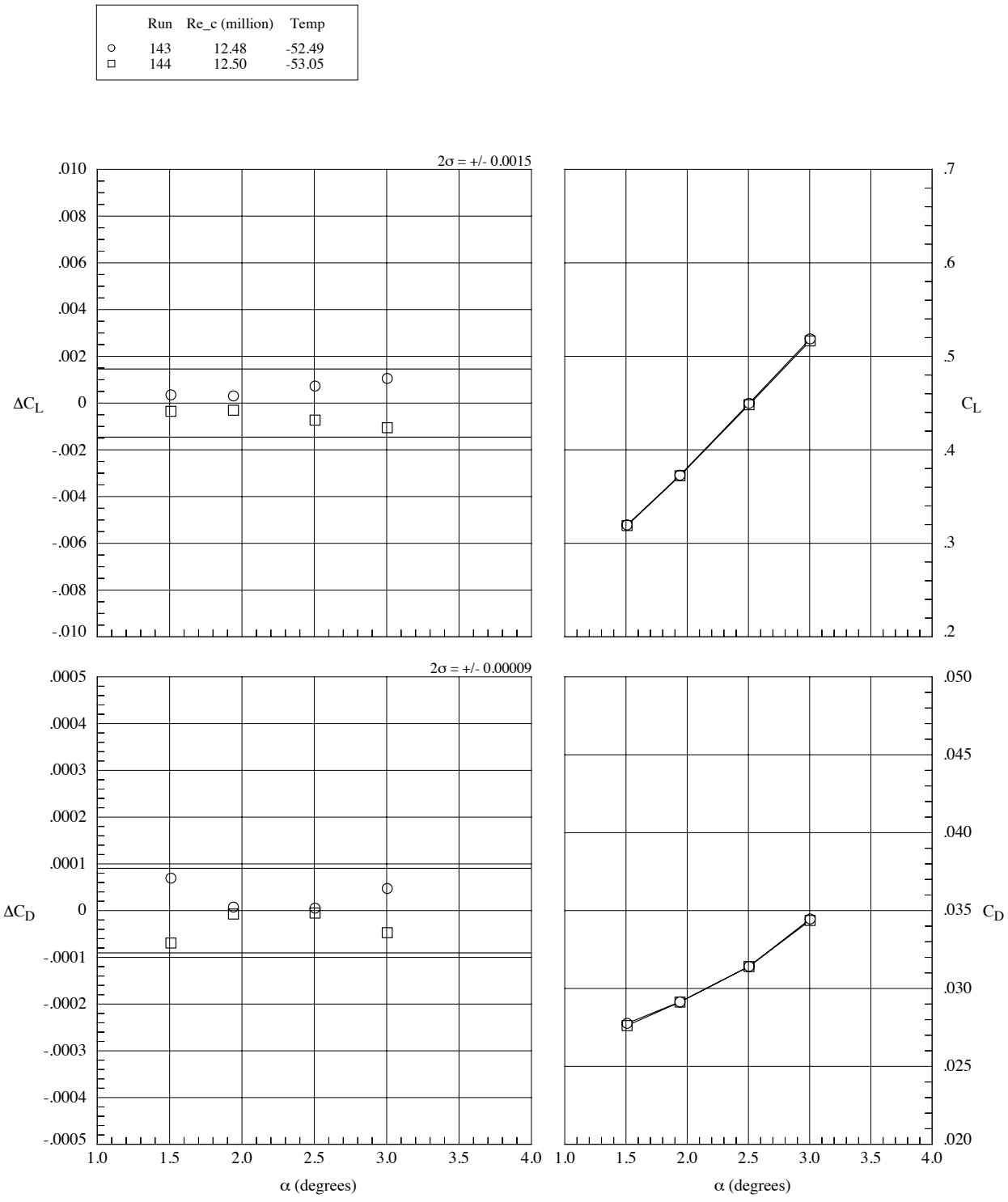

Fig. 13. Data repeatability, $M_\infty = 0.86$, $Re_c = 12.5$ million, $T_t = -53^\circ F$, $q_\infty = 1120$ psf. Solid line indicates 2-sigma limits based on the residual data.

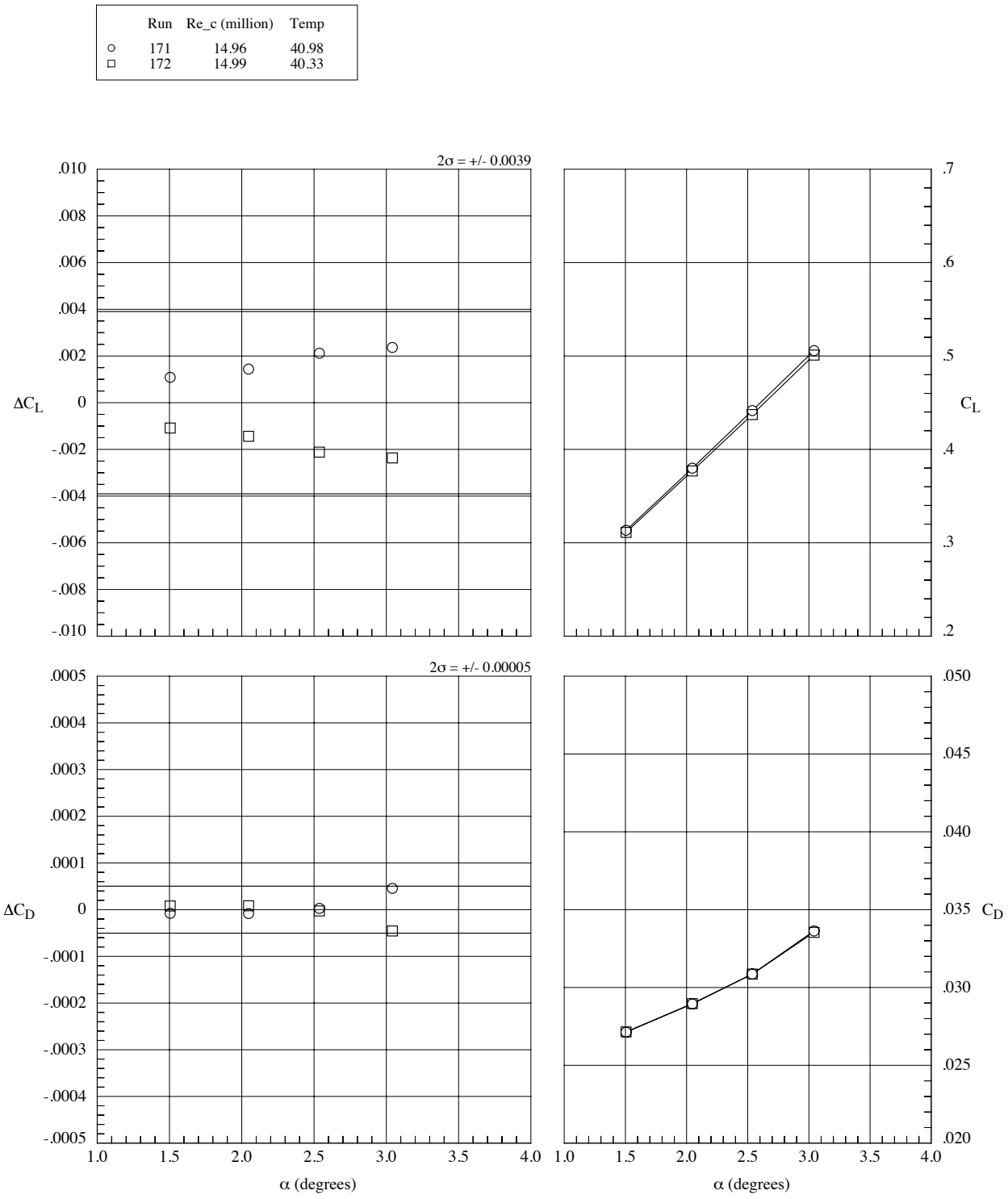

Fig. 14. Data repeatability, $M_\infty = 0.86$, $Re_c = 15$ million, $T_t = 40^\circ F$, $q_\infty = 1775$ psf. Solid line indicates 2-sigma limits based on the residual data.

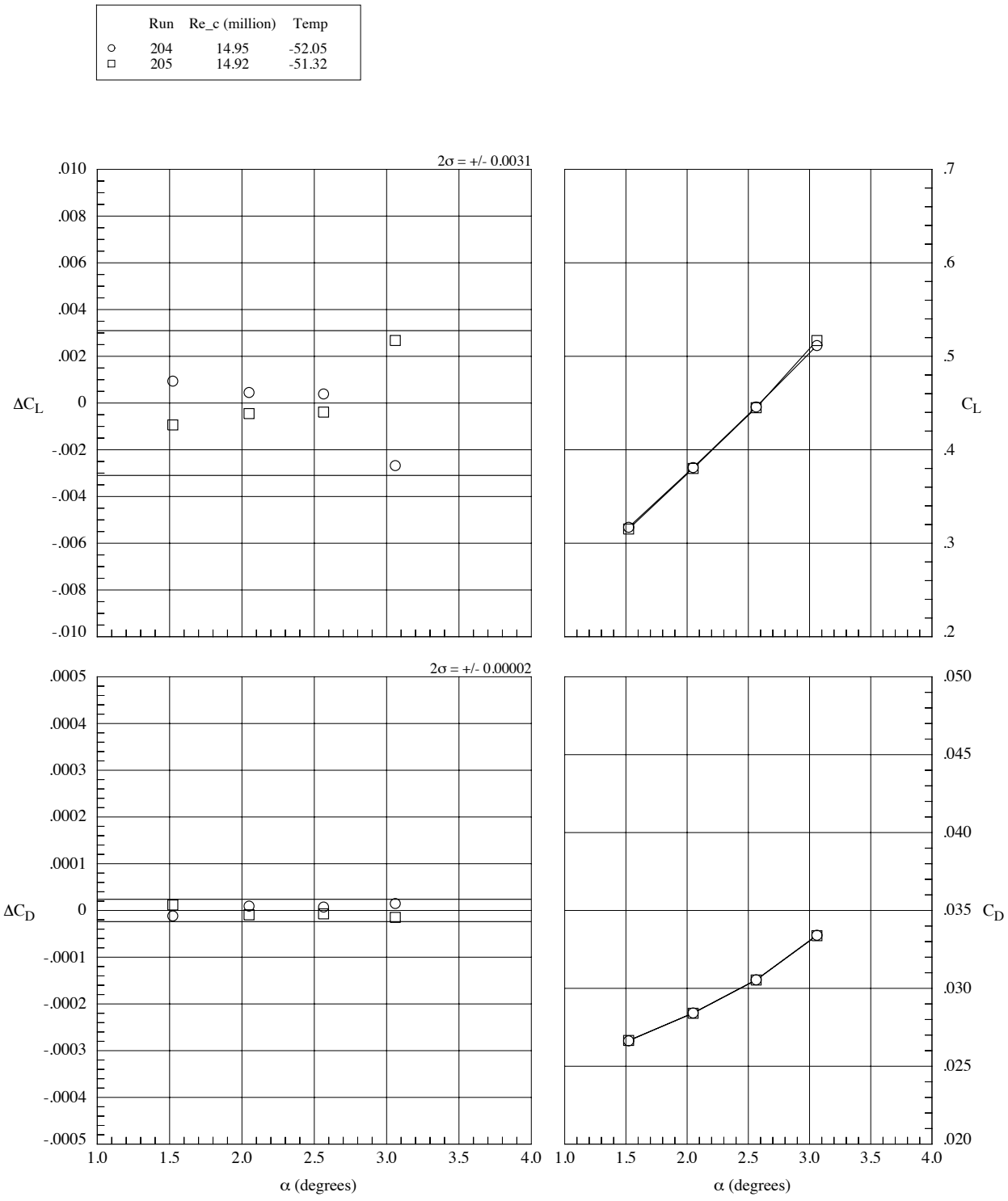

Fig. 15. Data repeatability, $M_\infty = 0.86$, $Re_c = 15$ million, $T_t = -53^\circ F$, $q_\infty = 1346$ psf. Solid line indicates 2-sigma limits based on the residual data.

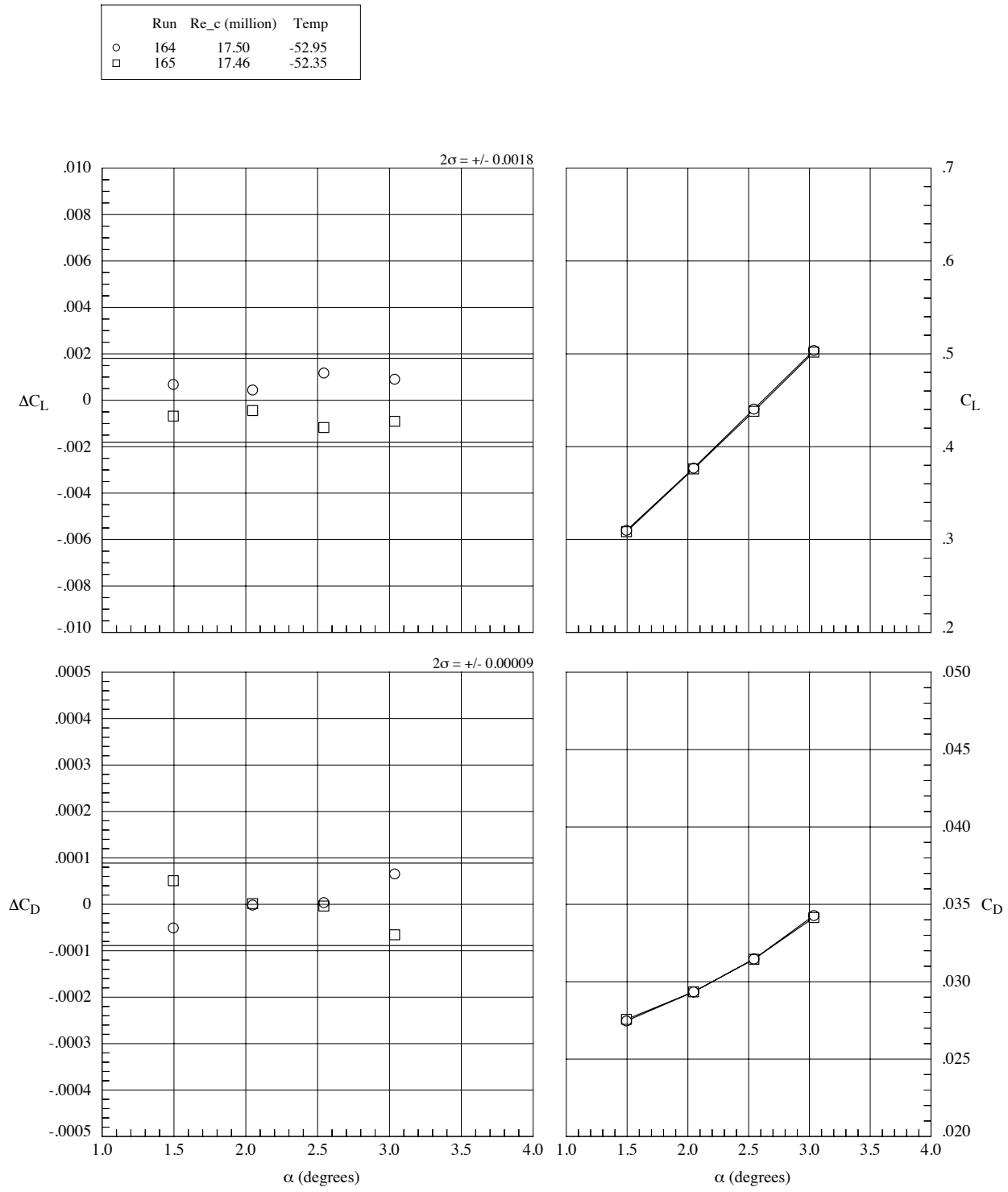

Fig. 16. Data repeatability, $M_\infty = 0.85$, $Re_c = 17.5$ million, $T_t = -53^\circ F$, $q_\infty = 1570$ psf. Solid line indicates 2-sigma limits based on the residual data.

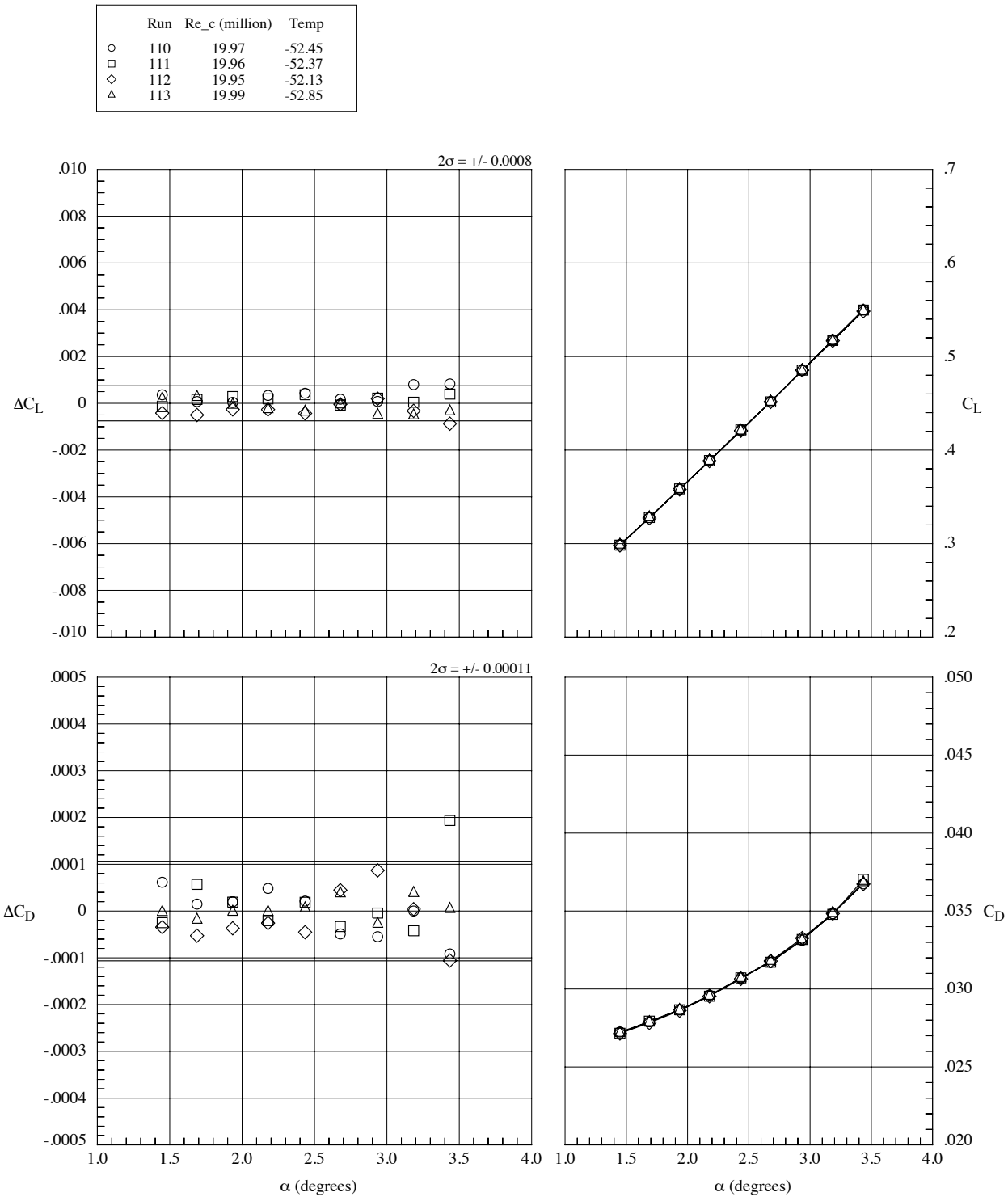

Fig. 17. Data repeatability, $M_\infty = 0.86$, $Re_c = 20$ million, $T_t = -53°F$, $q_\infty = 1795$ psf. Solid line indicates 2-sigma limits based on the residual data.

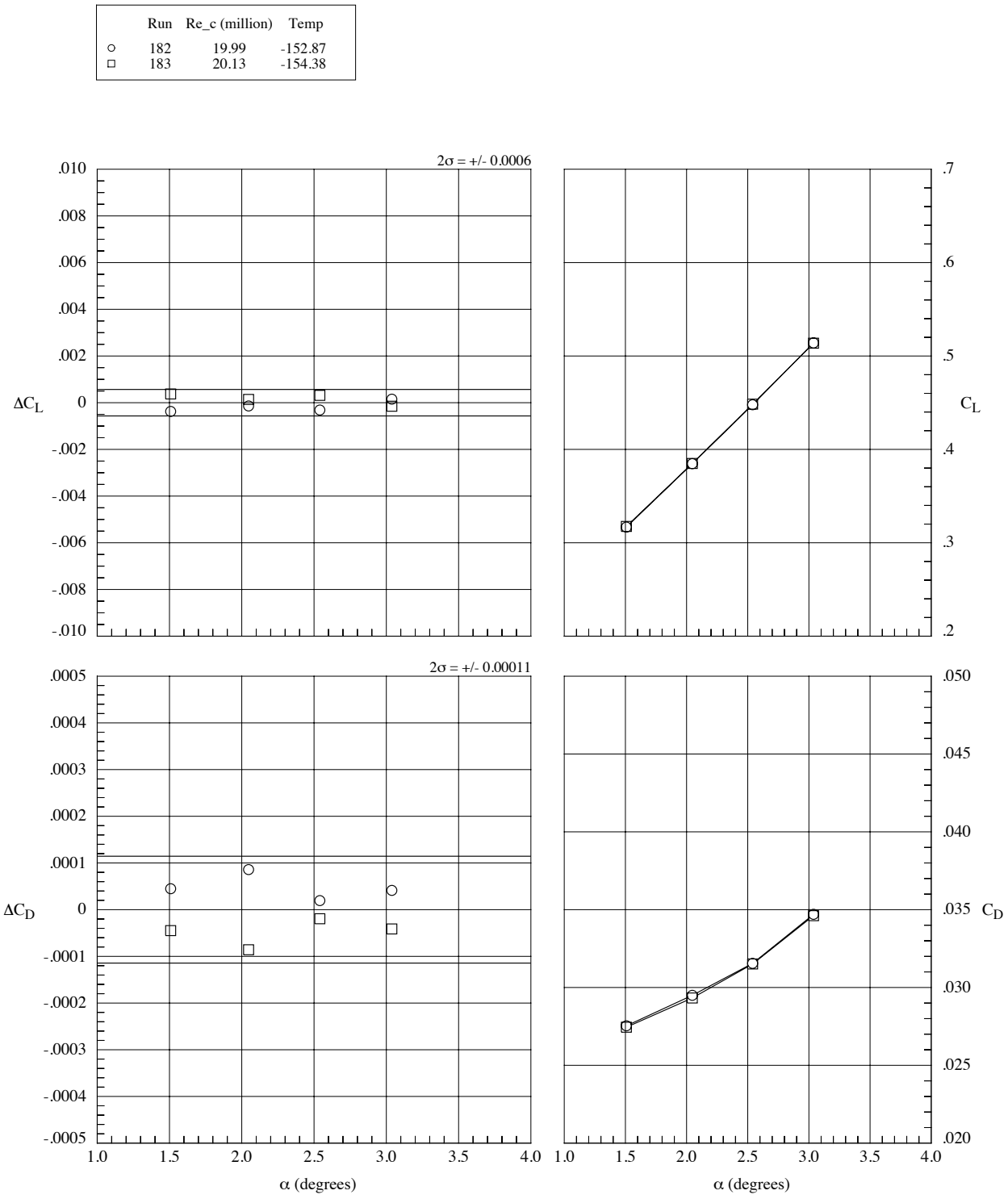

Fig. 18. Data repeatability, $M_\infty = 0.86$, $Re_c = 20$ million, $T_t = -153^\circ F$, $q_\infty = 1208$ psf. Solid line indicates 2-sigma limits based on the residual data.

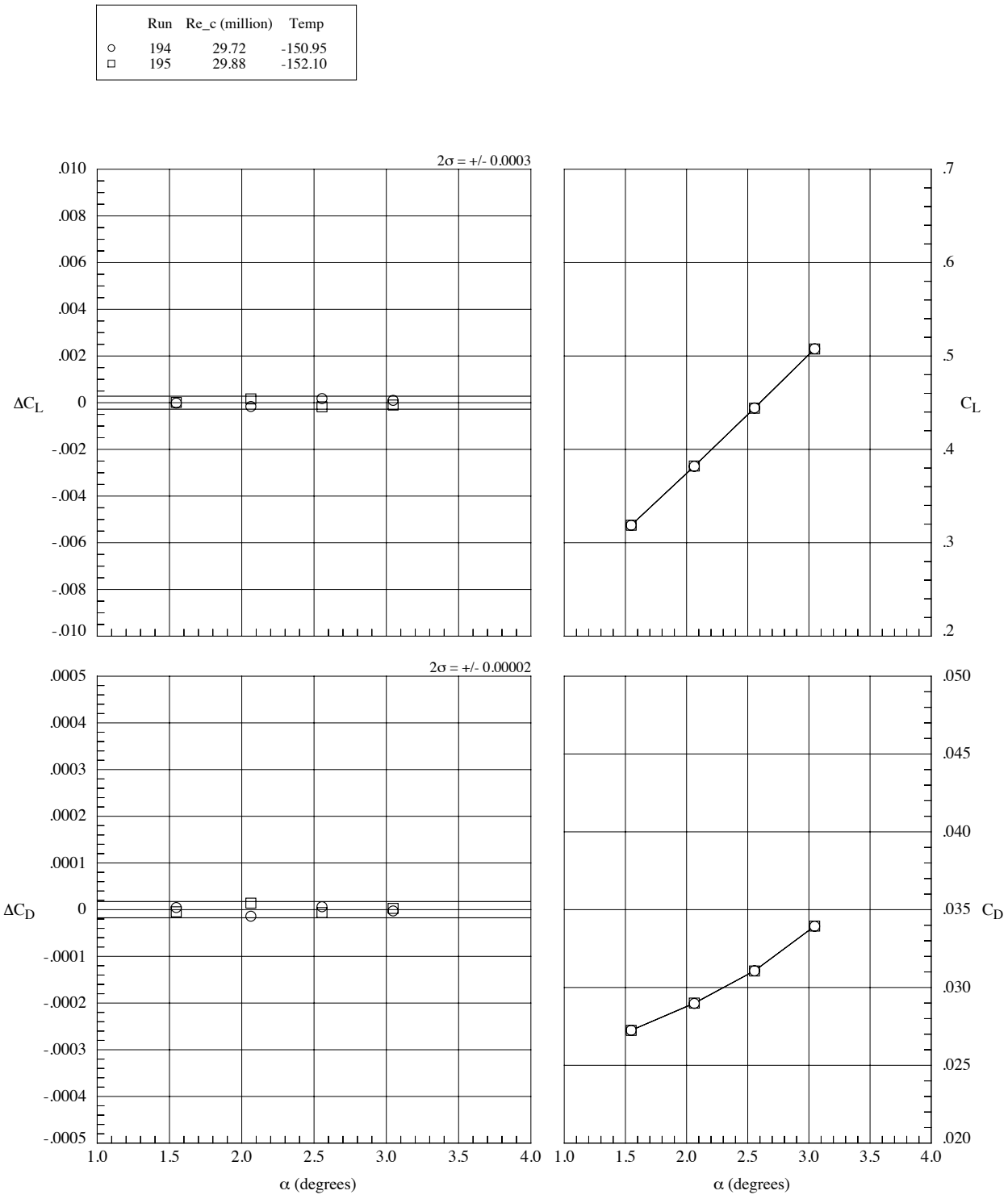

Fig. 19. Data repeatability, $M_\infty = 0.86$, $Re_c = 30$ million, $T_t = -153^\circ F$, $q_\infty = 1814$ psf. Solid line indicates 2-sigma limits based on the residual data.

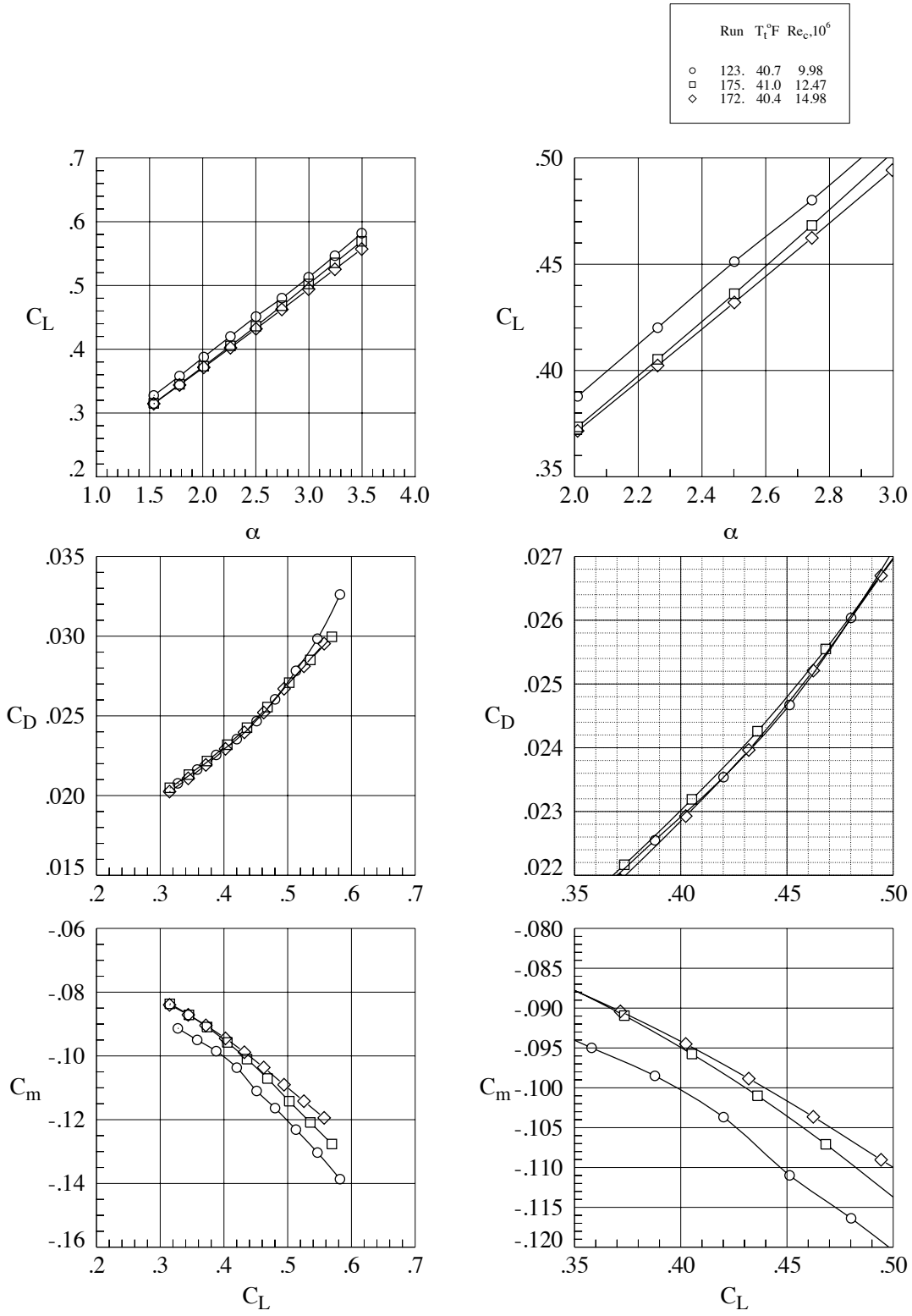

Fig. 20. Revnolds number effects, $M_\infty = 0.86$, $T_t = 40^\circ F$.

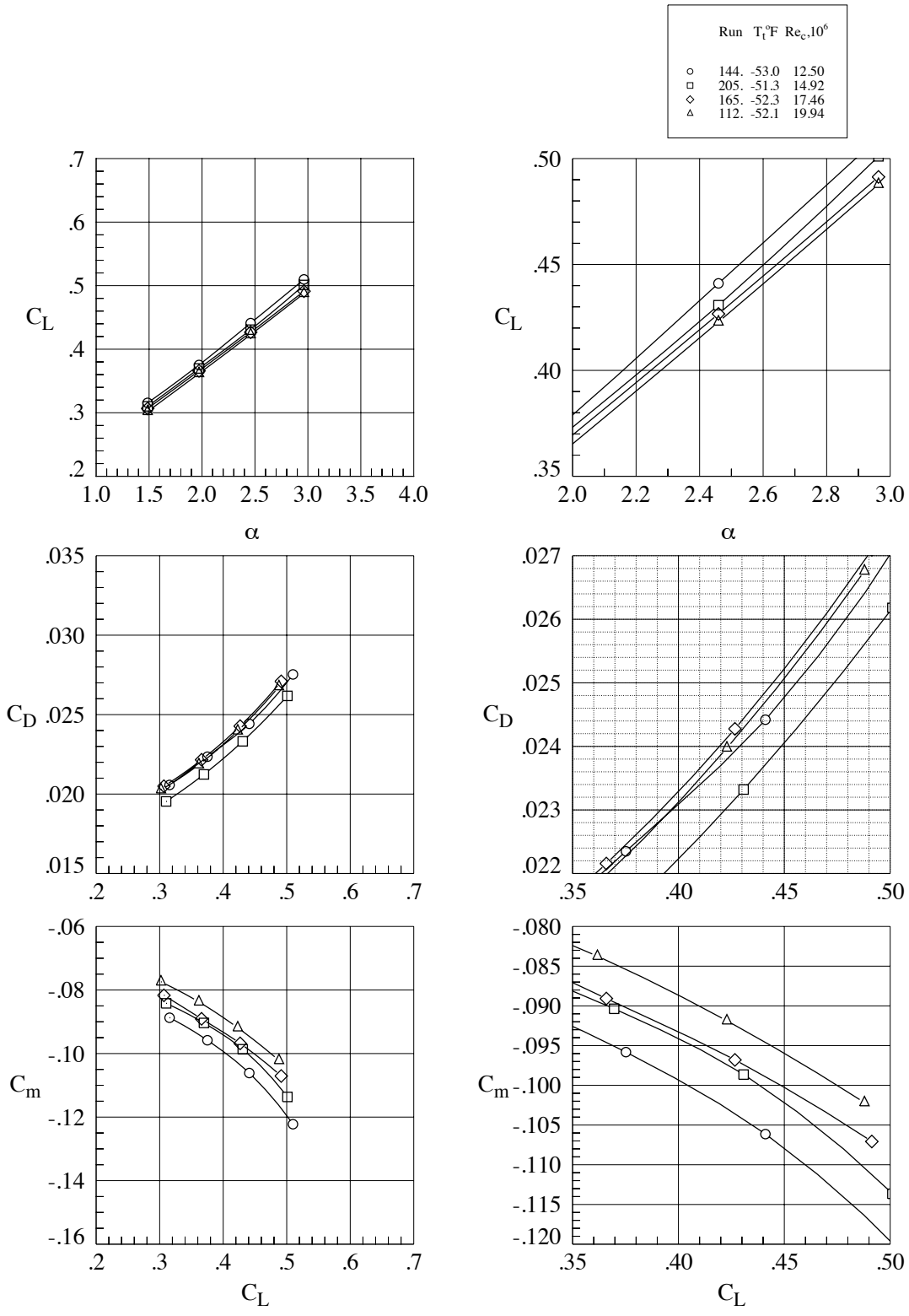

Fig. 21. Reynolds number effects, $M_\infty = 0.86$, $T_t = -53^\circ F$.

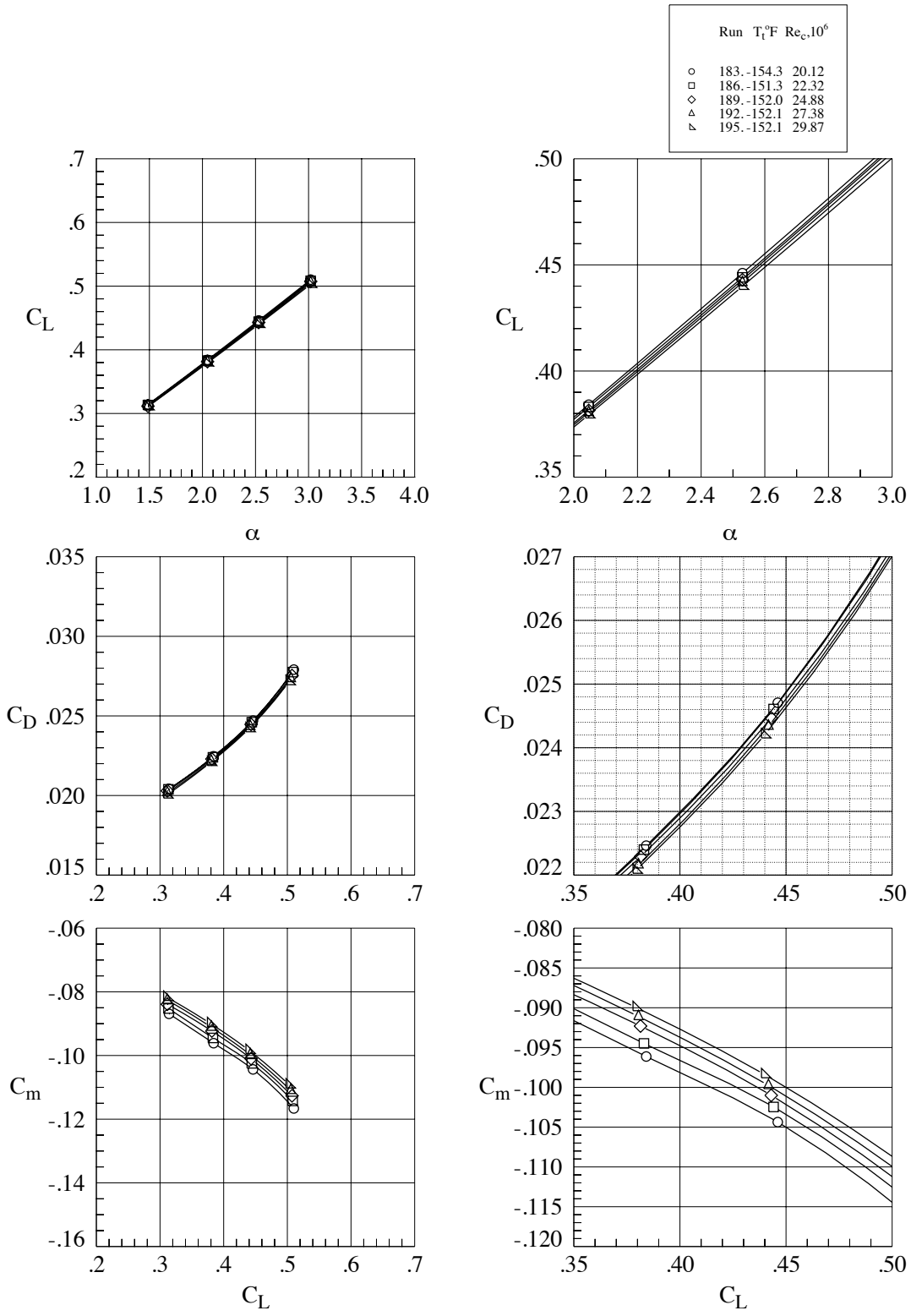

Fig. 22. Reynolds number effects, $M_\infty = 0.86$, $T_t = -153$°F.

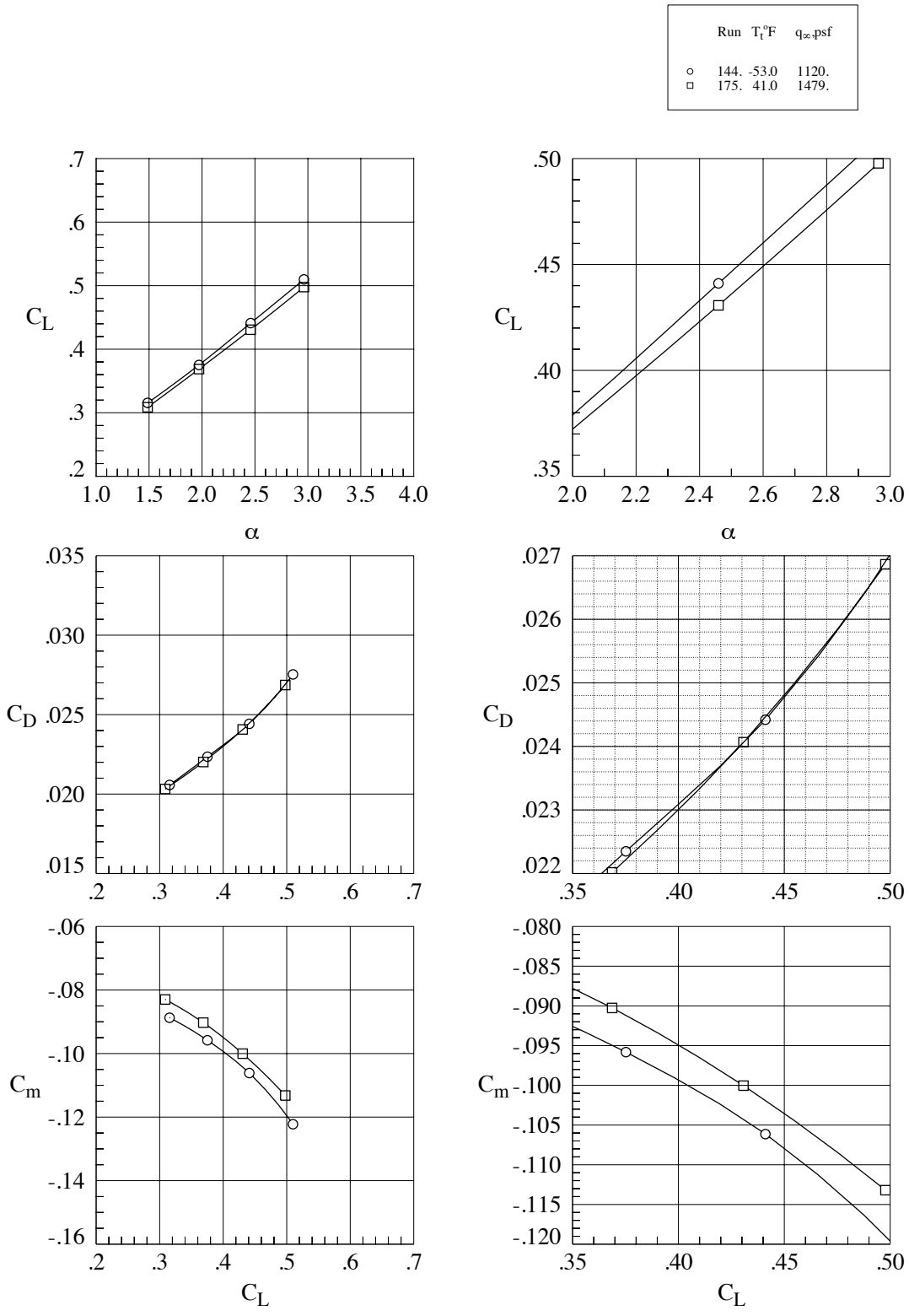

Fig. 23. Aeroelastic effects, $M_\infty = 0.86$, $Re_c = 12.5$ million.

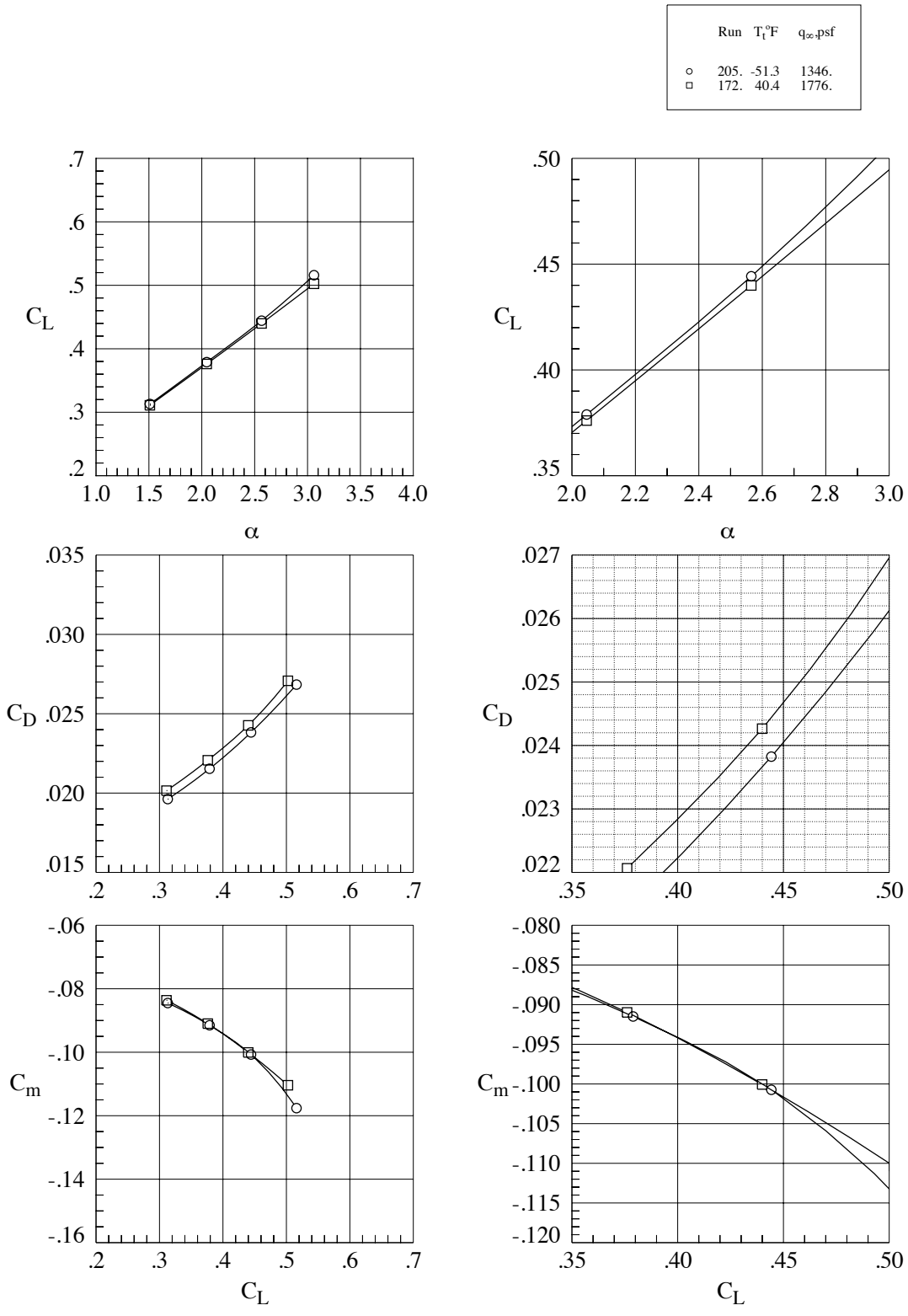

Fig. 24. Aeroelastic effects, $M_\infty = 0.86$, $Re_c = 15$ million.

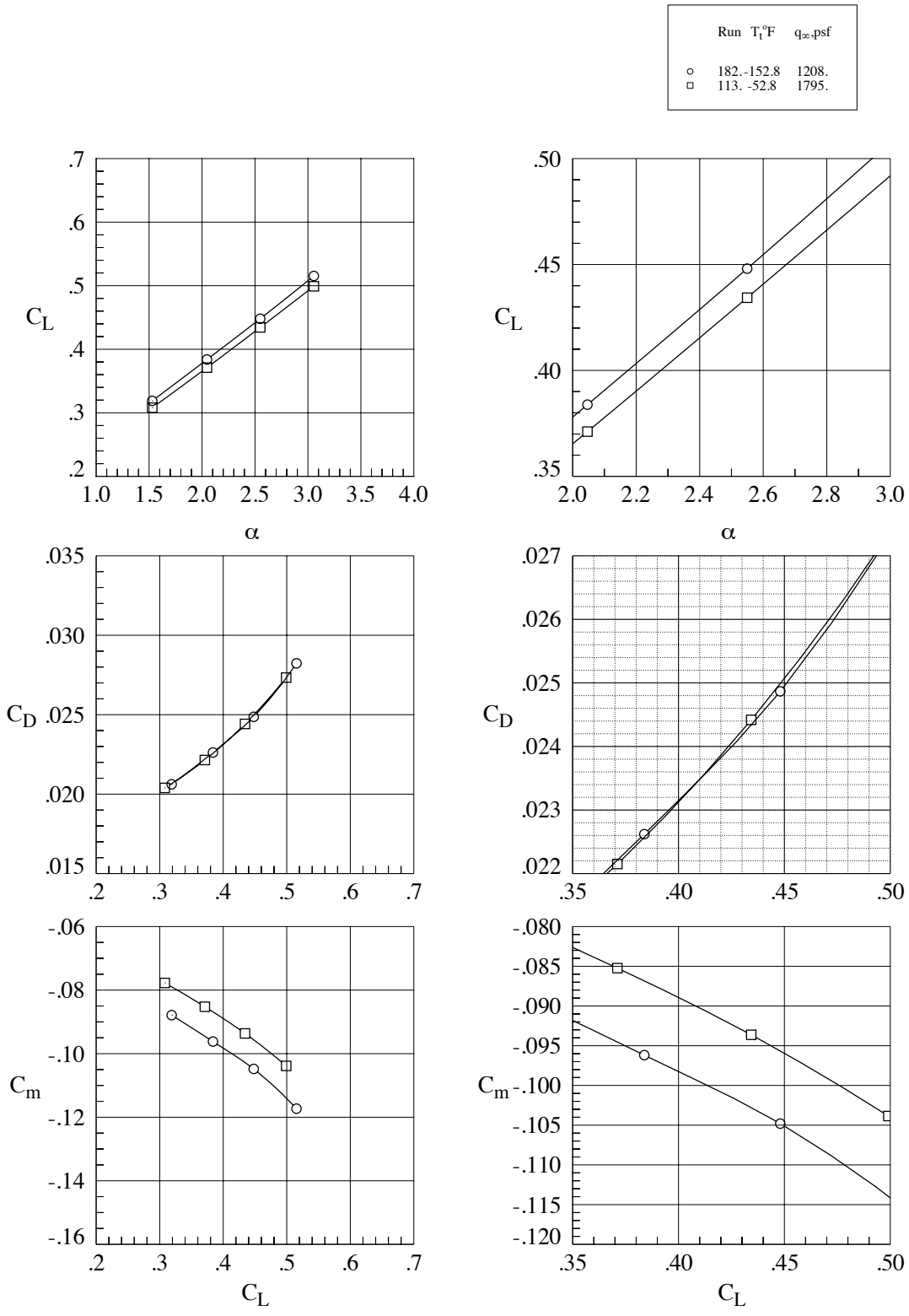

Fig. 25. Aeroelastic effects, $M_\infty = 0.86$, $Re_c = 20$ million.